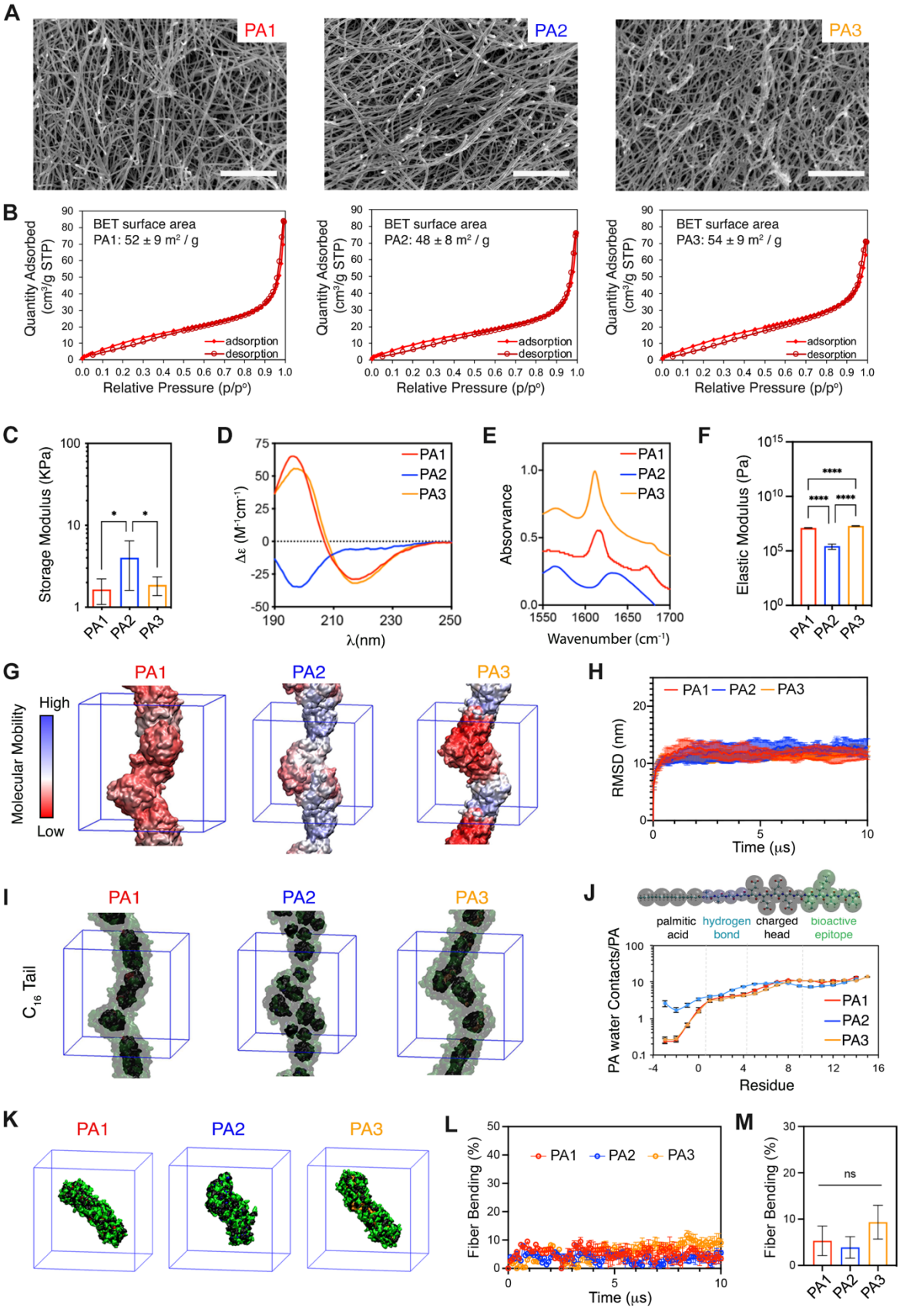
A
PA1
PA2
PA3
B
BET surface area
PA1: 52 ± 9 m² / g
PA2: 48 ± 8 m² / g
PA3: 54 ± 9 m² / g
Quantity Adsorbed (cm³/g STP)
adsorption
desorption
Relative Pressure (p/p°)
C
Storage Modulus (KPa)
D
Δε (M⁻¹cm⁻¹)
λ(nm)
E
Absorvance
Wavenumber (cm⁻¹)
F
Elastic Modulus (Pa)
****
G
Molecular Mobility
High
Low
H
RMSD (nm)
Time (μs)
I
C16 Tail
J
palmitic acid
hydrogen bond
charged head
bioactive epitope
PA water Contacts/PA
Residue
K
L
Fiber Bending (%)
Time (μs)
M
ns

Figure S1, related to Figure 1. Characterization of IKVAV-PA Supramolecular Nanofibers with Different Degrees of Supramolecular Motion.

(**A**) SEM micrographs of PA**1**, PA**2**, and PA**3** coatings. Scale bar =2 μm.

(**B**) Line graphs displaying nitrogen physisorption isotherms of IKVAV-PA scaffolds composed of PA**1** (left), PA**2** (middle), and PA3 (right). The BET specific surface areas are calculated between 0.05 < p/p0 < 0.35 (see Methods).

(**C**) Bar graph displaying the storage modulus of PA**1**, PA**2,** and PA**3** gels. Asterisks represent significant differences based on ANOVA followed by Tukey's multiple comparison test; *P<0.05.

(**D**) Line graph showing the circular dichroism (CD) spectra of PA**1**, PA**2,** and PA**3** nanofibers.

(**E**) Line graph showing the Fourier-transform infrared spectroscopy (FTIR) spectra of PA**1**, PA**2,** and PA**3** nanofibers.

(**F**) Bar graph displaying the elastic modulus of PA**1**, PA**2,** and PA**3** fibers. Asterisks represent significant differences based on ANOVA followed by Tukey's multiple comparison test; ****P<0.0001.

(**G**) Self-assembled structures of single PA**1**, PA**2,** and PA**3** nanofibers after 10 μs of coarse-grained molecular dynamic simulations. Colors correspond to the molecular mobility in the last 5 μs accounted with RMSF. The illustrations include partial periodic images through the fiber formation axis. The simulation box is shown in blue, and water and ions are omitted for clarity.

(**H**) Line graph representing the root mean square deviation (RMSD) *vs*. time of PA**1**, PA**2**, and PA**3**. The RMSD plots are the average of 5 independent simulations.

(**I**) Self-assembled structures of single fibers of PA**1**, PA**2**, and PA**3** after 10 μs of coarse-grained molecular dynamic simulations. PA molecules are shown in transparent grey, except for the C_{16} tail represented in black. The illustrations include partial periodic images through the fiber formation axis. The simulation box is shown in blue, and water and ions are omitted for clarity.

(**J**) Water mapping analysis of PA**1**, PA**2,** and PA**3** within the assemblies through the last 2 μs of simulation averaging the contacts of each of the PA beads (C_{16} tail beads numbered -3 to 0 and peptide backbone beads numbered from 1 on) with water. Results represent data obtained from 5 independent simulations. Chemical structure of IKVAV-PA sequence is represented on top.

(**K**) Non-periodic PA**1**, PA**2,** and PA**3** nanofibers after 10 μs of coarse-grained molecular dynamic simulations. The simulation box is shown in blue, and water and ions are omitted for clarity.

(**L**) Line graph representing the percentage of bending *vs*. time of PA**1**, PA**2**, and PA**3** nanofibers**.** The percentage of bending plots are the average of 3 independent simulations.

(**M**) Bar graph depicting the percentage of bending of PA**1**, PA**2**, and PA**3** nanofibers**.** The plots are the average of 3 independent simulations; ns: no significant differences based on ANOVA followed by Tukey's multiple comparison test.

All the values are presented as the mean ± SD.

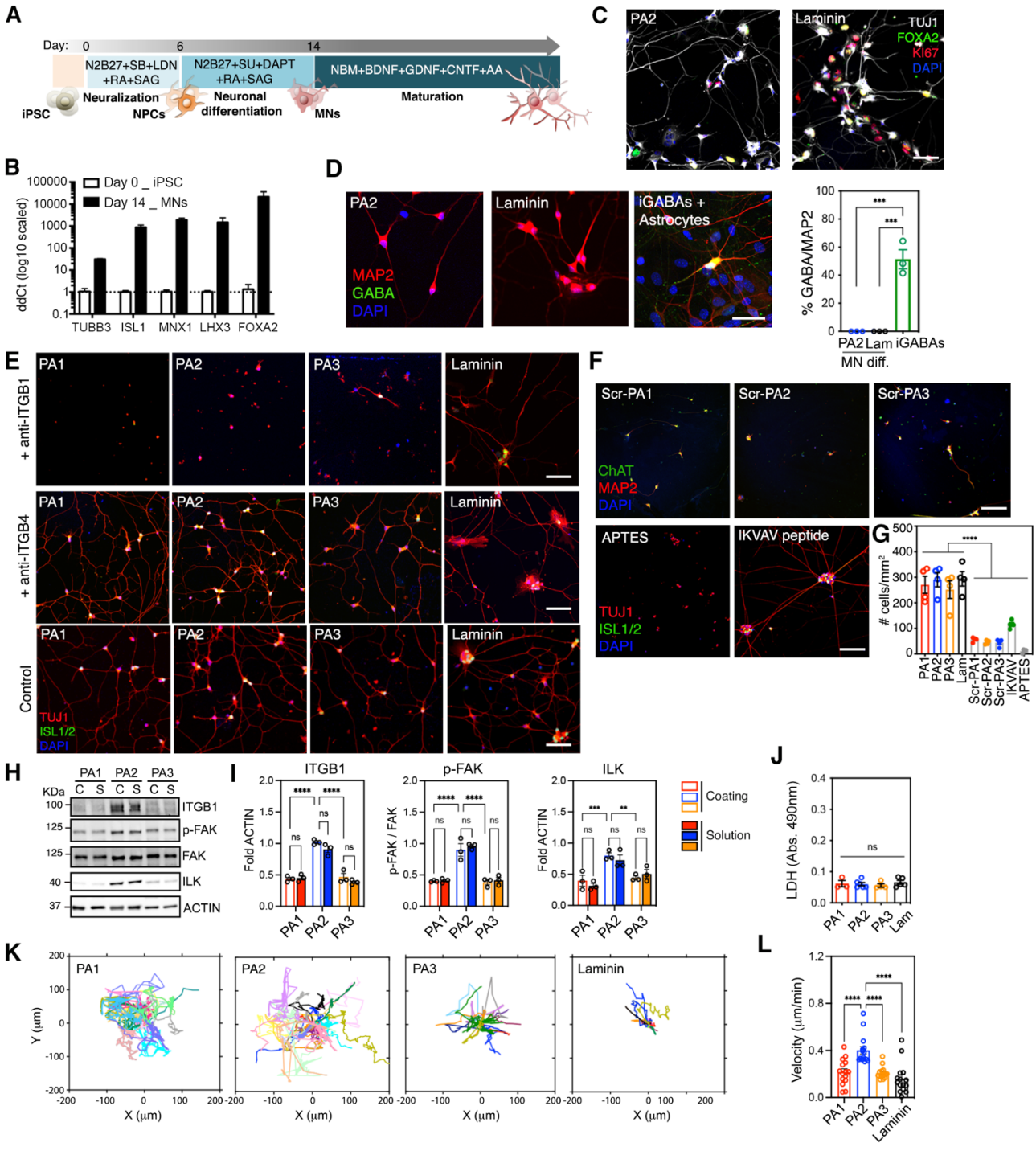
A
Day: 0 6 14
N2B27+SB+LDN +RA+SAG
N2B27+SU+DAPT +RA+SAG
NBM+BDNF+GDNF+CNTF+AA
iPSC
Neuralization
NPCs
Neuronal differentiation
MNs
Maturation
B
Day 0 _ iPSC
Day 14 _ MNs
ddCt (log10 scaled)
TUBB3 ISL1 MNX1 LHX3 FOXA2
C
PA2
Laminin
TUJ1
FOXA2
KI67
DAPI
D
PA2
MAP2
GABA
DAPI
Laminin
iGABAs + Astrocytes
% GABA/MAP2
PA2 Lam iGABAs
MN diff.
E
+ anti-ITGB1
+ anti-ITGB4
Control
PA1
PA2
PA3
Laminin
TUJ1
ISL1/2
DAPI
F
Scr-PA1
Scr-PA2
Scr-PA3
ChAT
MAP2
DAPI
APTES
IKVAV peptide
TUJ1
ISL1/2
DAPI
G
cells/mm²
PA1 PA2 PA3 Lam Scr-PA1 Scr-PA2 Scr-PA3 IKVAV APTES
H
KDa
C S C S C S
PA1 PA2 PA3
ITGB1
p-FAK
FAK
ILK
ACTIN
I
ITGB1
p-FAK
ILK
Fold ACTIN
p-FAK / FAK
Coating
Solution
PA1 PA2 PA3
J
LDH (Abs. 490nm)
PA1 PA2 PA3 Lam
K
PA1
PA2
PA3
Laminin
Y (µm)
X (µm)
L
Velocity (µm/min)
PA1 PA2 PA3 Laminin

Figure S2, related to Figure 2. Highly Mobile IKVAV-PA Supramolecular Scaffold Enhances Integrin-Dependent Effects on hiPSC-Derived MNs.

(**A**) Schematic representation of the 14-day protocol of MN differentiation from human hiPSC that is utilized in this study.

(**B**) Bar graph displaying the RNA expression levels of neuronal (TUBB3), MN (ISL1, MNX1 and LHX3) and non-neuronal/floor plate (FOXA2) markers at day 0 (hiPSC cultures; white bars) and day 14 (highly MN differentiated cultures; black bars) as measured by qRT-PCR. Data was normalized to day 0 values.

(**C**) Fluorescence microscopy images of hiPSC-derived MN cultures on PA**2** and laminin coatings stained for TUJ1 (white), KI67 (red) and FOXA2 (green). Nuclei were labeled with DAPI (blue).

(**D**) Left: Representative confocal micrographs of hiPSC-derived MN cultures on PA**2** and laminin coatings stained for MAP2 (red) and GABA (green). Nuclear DNA is stained with DAPI (blue). Human GABAergic interneurons cultured on mouse astrocytes were used as a positive control for GABA staining. Right: Bar graph representing the percentage of GABA/MAP2 positive cells in hiPSC-derived MN cultures on the different conditions tested. Asterisks represent significant differences based on ANOVA followed by Tukey's multiple comparison; ***P<0.001.

(**E**) Representative confocal micrographs of MNs treated with anti-ITGB1- or anti-ITGB4-blocking antibodies and cultured on different IKVAV-PA or laminin coatings for 72h. Cells were stained with neuronal (TUJ1, red) and MN (ISL1/2, green) markers, and nuclei were stained with DAPI (blue).

(**F**) Representative confocal images of hiPSC-derived MNs cultured on the scrambled VVIAK-PAs (Scr-PA**1**, -PA**2** and -PA**3**)**,** APTES, and IKVAV peptide coatings. MNs were immunolabeled for neuronal (MAP2, TUJ1; red) and MN (ChAT, ISL1/2; green) markers. Nuclei were stained with DAPI (blue).

(**G**) Bar graph representing the number of cells per mm^2 cultured on scrambled VVIAK-PAs (Scr-PA**1**, -PA**2** and -PA**3**)**,** APTES, and immobilized IKVAV. The IKVAV-PA**1**, PA**2** and PA**3**, as well as a commercial laminin coating were used as references. Asterisks represent significant differences based on ANOVA followed by Tukey's multiple comparison test; ****P<0.0001.

(**H**) Representative western blot (WB) of ITGB1, p-FAK, FAK and ILK in MNs cultured with different IKVAV-PAs in solution (S) or coatings (C) for 72h. ACTIN was used as a loading control.

(**I**) Bar graphs representing the normalized protein levels of ITGB1, p-FAK, and ILK in MNs cultured with different IKVAV-PAs in solution (S) or coatings (C) for 72h. Asterisks represent significant differences based on ANOVA followed by Tukey's multiple comparison test; **P <0.01, ***P<0.001, and ****P<0.0001; ns: no significant differences.

(**J**) Bar graph representing the released LDH levels in hiPSC-derived MN cultures after 72h in PA**1**, PA**2**, PA**3** and commercial laminin coatings. ns: no significant differences based on ANOVA followed by Tukey's multiple comparison test.

(**K**) XY-trajectory plots displaying the migratory paths of individual human hiPSC-derived MNs over 72h on IKVAV-PAs or commercial laminin coatings.

(**L**) Bar graph displaying migration velocity of hiPSC-derived MNs plated on various coatings as shown in **N**. Asterisks represent significant differences based on ANOVA followed by Tukey's multiple comparison test; ****P<0.0001.

Data was obtained from at least 2-3 independent differentiations. All the values are presented as the mean ± SEM; Each dot in the graphs represents average values of multiple fields from a specific differentiation in **D**, **G**, and **J;** unique values from independent differentiations in **I**; and an individual cell in **L**. Scale bars: **C**=50 μm**; D**=40 μm; **E** and **F**=100 μm.

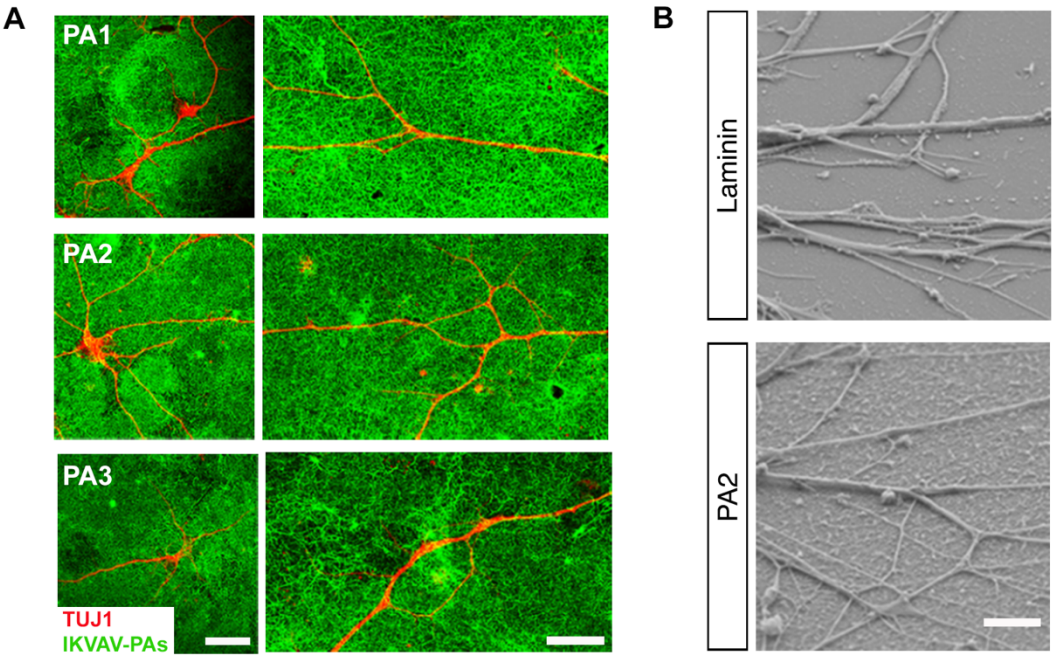
A
PA1
PA2
PA3
TUJ1
IKVAV-PAs
B
Laminin
PA2

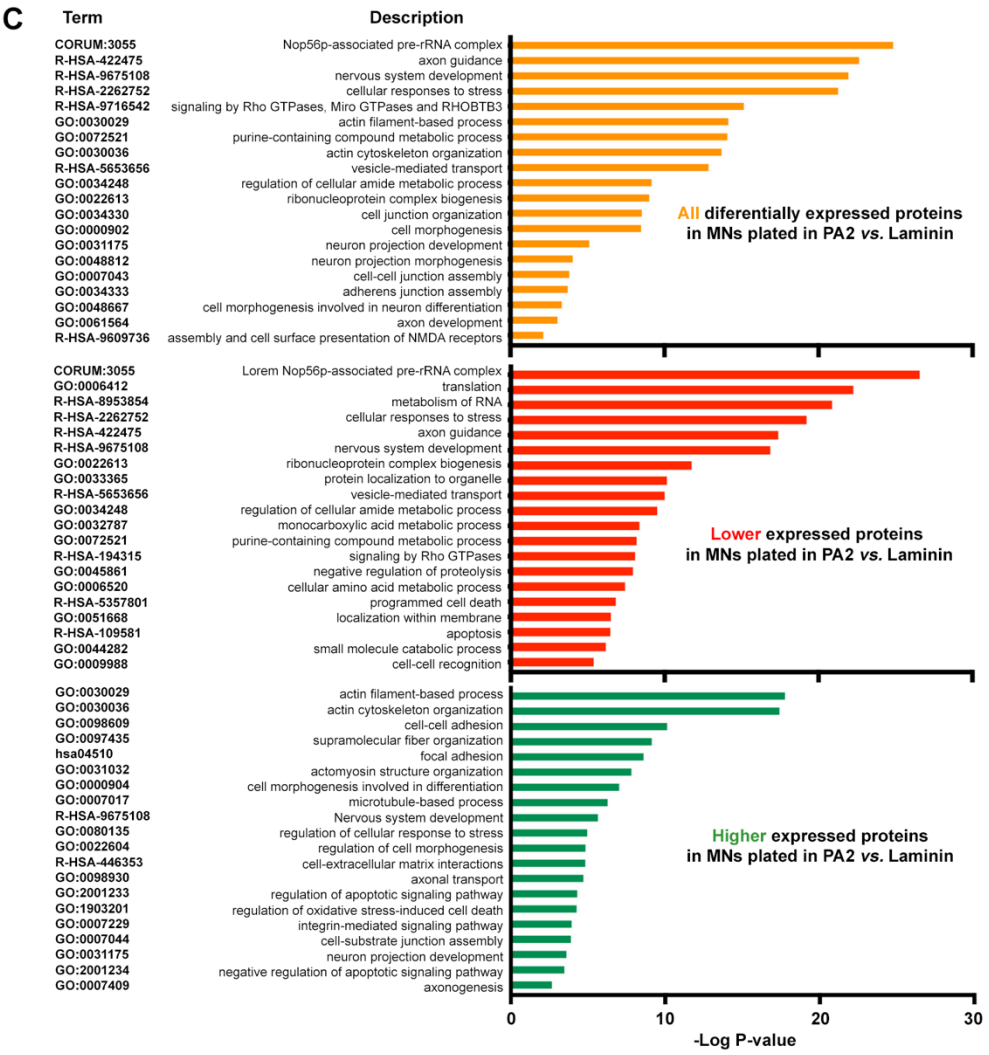
C
Term
Description
CORUM:3055 Nop56p-associated pre-rRNA complex
R-HSA-422475 axon guidance
R-HSA-9675108 nervous system development
R-HSA-2262752 cellular responses to stress
R-HSA-9716542 signaling by Rho GTPases, Miro GTPases and RHOBTB3
GO:0030029 actin filament-based process
GO:0072521 purine-containing compound metabolic process
GO:0030036 actin cytoskeleton organization
R-HSA-5653656 vesicle-mediated transport
GO:0034248 regulation of cellular amide metabolic process
GO:0022613 ribonucleoprotein complex biogenesis
GO:0034330 cell junction organization
GO:0000902 cell morphogenesis
GO:0031175 neuron projection development
GO:0048812 neuron projection morphogenesis
GO:0007043 cell-cell junction assembly
GO:0034333 adherens junction assembly
GO:0048667 cell morphogenesis involved in neuron differentiation
GO:0061564 axon development
R-HSA-9609736 assembly and cell surface presentation of NMDA receptors
All diferentially expressed proteins in MNs plated in PA2 vs. Laminin
CORUM:3055 Lorem Nop56p-associated pre-rRNA complex
GO:0006412 translation
R-HSA-8953854 metabolism of RNA
R-HSA-2262752 cellular responses to stress
R-HSA-422475 axon guidance
R-HSA-9675108 nervous system development
GO:0022613 ribonucleoprotein complex biogenesis
GO:0033365 protein localization to organelle
R-HSA-5653656 vesicle-mediated transport
GO:0034248 regulation of cellular amide metabolic process
GO:0032787 monocarboxylic acid metabolic process
GO:0072521 purine-containing compound metabolic process
R-HSA-194315 signaling by Rho GTPases
GO:0045861 negative regulation of proteolysis
GO:0006520 cellular amino acid metabolic process
R-HSA-5357801 programmed cell death
GO:0051668 localization within membrane
R-HSA-109581 apoptosis
GO:0044282 small molecule catabolic process
GO:0009988 cell-cell recognition
Lower expressed proteins in MNs plated in PA2 vs. Laminin
GO:0030029 actin filament-based process
GO:0030036 actin cytoskeleton organization
GO:0098609 cell-cell adhesion
GO:0097435 supramolecular fiber organization
hsa04510 focal adhesion
GO:0031032 actomyosin structure organization
GO:0000904 cell morphogenesis involved in differentiation
GO:0007017 microtubule-based process
R-HSA-9675108 Nervous system development
GO:0080135 regulation of cellular response to stress
GO:0022604 regulation of cell morphogenesis
R-HSA-446353 cell-extracellular matrix interactions
GO:0098930 axonal transport
GO:2001233 regulation of apoptotic signaling pathway
GO:1903201 regulation of oxidative stress-induced cell death
GO:0007229 integrin-mediated signaling pathway
GO:0007044 cell-substrate junction assembly
GO:0031175 neuron projection development
GO:2001234 negative regulation of apoptotic signaling pathway
GO:0007409 axonogenesis
Higher expressed proteins in MNs plated in PA2 vs. Laminin
0
10
20
30
-Log P-value

Figure S3, related to Figure 3. Unbiased Characterization of the Effects of IKVAV-PA Nanofibers with High Supramolecular Motion on Long-Term hiPSC-Derived MN Cultures.

(**A**) Left: Structured illumination micrographs of TUJ1+ hiPSC-derived MNs cultured on different IKVAV-PAs covalently linked to alexa-488 dye after 60 days *in vitro*. Right: Higher magnification of the neuronal processes on the different IKVAV-PA coatings.

(**B**) SEM micrographs of hiPSC-derived MN processes cultured on commercial laminin coating or on IKVAV-PA**2** nanofibers after 60 days *in vitro*.

(**C**) Bar plots displaying the most representative GO terms found enriched among all the differentially expressed proteins (orange) as well as the group of proteins downregulated (red) or upregulated (green) in MN cultures plated for >45 days on PA**2** relative to MNs cultured on commercial laminin coatings.

Scale bars: **A**-Left=10 μm, **A-**Right=5 μm, and **B**=5 μm.

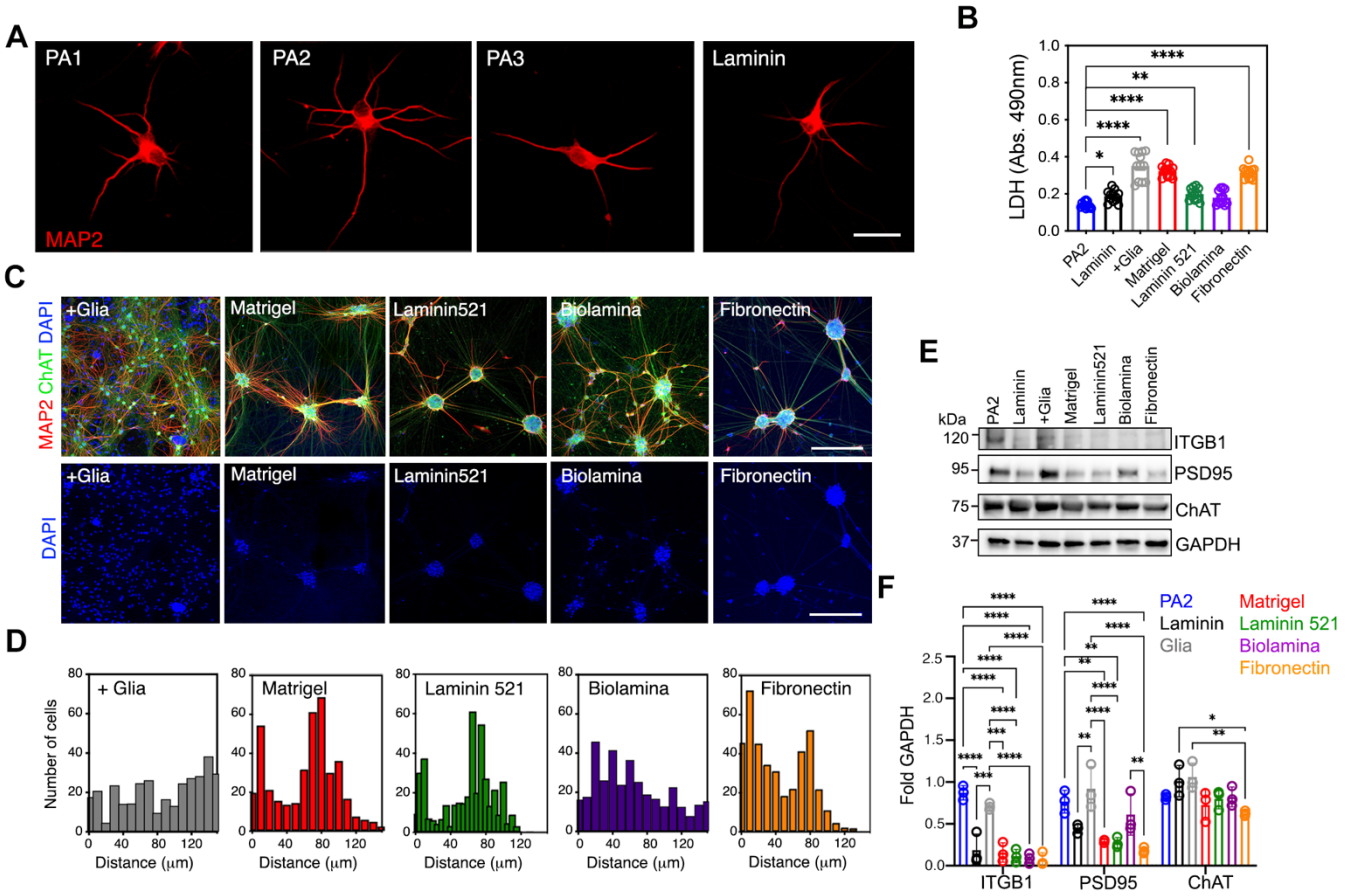

Figure S4, related to Figure 4. The Effect of IKVAV-PA Nanofibers with High Supramolecular Motion on Long-Term Survival, Adhesion and Neuronal Morphogenesis on hiPSC-Derived MN Cultures.

(**A**) Representative confocal micrographs of hiPSC-derived MNs on the different supramolecular IKVAV-PA coatings or laminin coatings for 45 days *in vitro*. Cells were stained with the dendritic marker, microtubule associated protein-2 (MAP2, red).

(**B**) Bar graph representing the released LDH levels in hiPSC-derived MN cultures plated on different ECM coatings (i.e., Mouse glia, Matrigel, Laminin 521, Biolamina, and Fibronectin) at day 45. Asterisks represent significant differences respect to PA**2** based on ANOVA followed by Tukey's multiple comparison test; *P<0.05, **P<0.01, ****P<0.0001.

(**C**) Representative confocal micrographs of hiPSC-derived MN cultures plated on different ECM coatings (i.e., Mouse glia, Matrigel, Laminin 521, Biolamina, and Fibronectin) at day 45. Cells were stained with the neuronal (MAP2, red) and MN (ChAT, green) markers (top row). Nuclei were stained with DAPI (blue).

(**D**) Histogram analysis of cell distribution on the different coatings referred on **E**.

(**E**) WB of ITGB1, PSD95, and ChAT protein levels in hiPSC-derived MNs cultured on the different coatings referred on **E**. GAPDH was used as a loading control.

(**F**) Bar plot showing the normalized levels of ITGB1, PSD95, and ChAT in the various coatings (PA2, Laminin, Mouse glia, Matrigel, Laminin 521, Biolamina and Fibronectin) at day 45. All values were normalized to GAPDH. Asterisks represent significant differences based on ANOVA followed by Tukey's multiple comparison test; *P<0.05, **P<0.01, ***P<0.001, ****P<0.0001.

Data was obtained from 2 independent differentiations. All the values are presented as the mean ± SEM. Each dot in the graphs represents individual values from distinct differentiations in **B** and **F**. Scale bars: **A**=25 μm; **C**=100 μm.

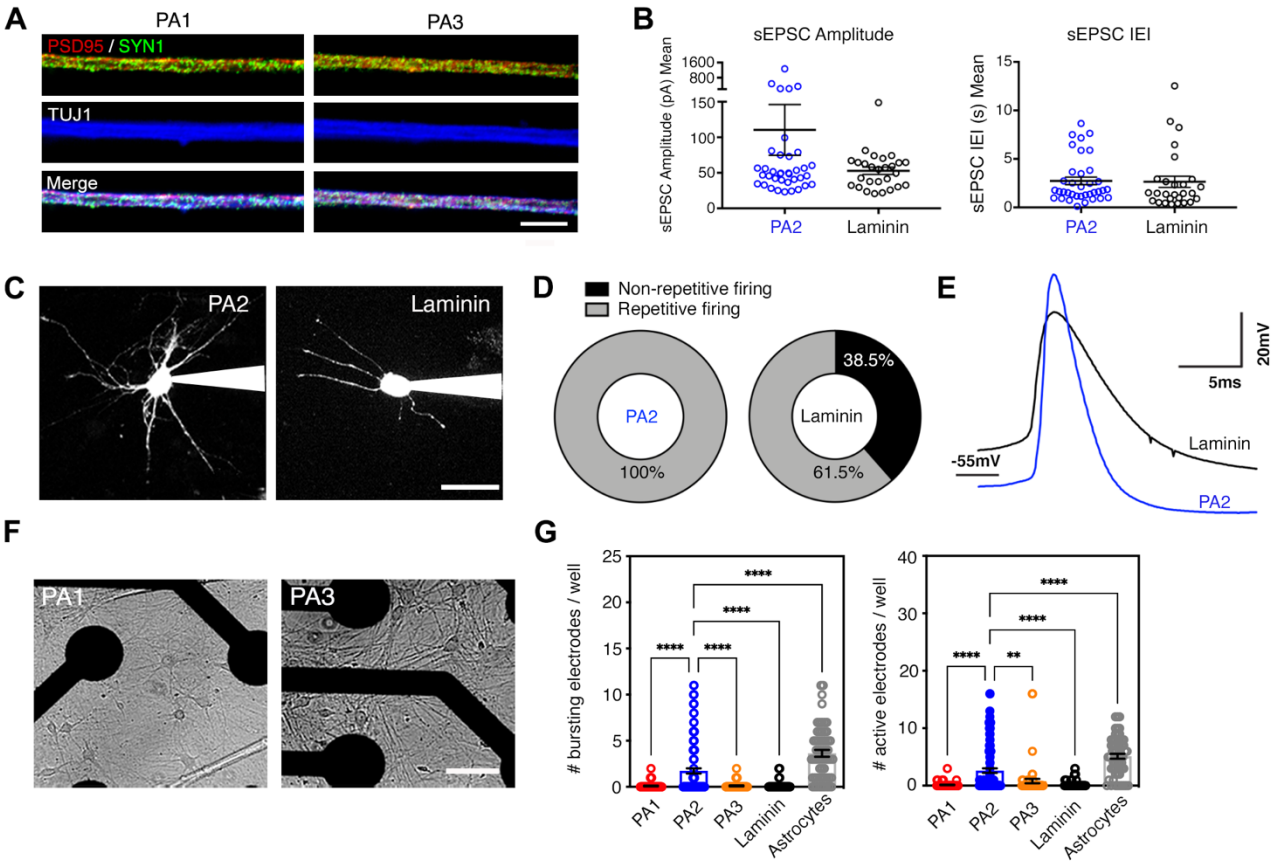

Figure S5 related to Figure 5. The Effect of Highly Mobile IKVAV-PA2 on Functional Neuronal Maturation.

(**A**) Representative SIM micrographs of pre- and post-synaptic terminals (labeled with SYN1 and PSD95, respectively) distributed along the hiPSC-derived MNs neurites cultured on IKVAV-PA**1** and PA**3** at day 60.

(**B**) Dot plots showing mean cell values of sEPSC amplitude (left) and IEI (right) from multiple hiPSC-derived MNs cultured on PA**2** (n=27) or laminin (n=37) coatings. No significant differences were observed between conditions based on a t-test.

(**C**) 2-photon microscopy images of hiPSC-derived MNs cultured on IKVAV-PA**2** and laminin coatings at days 48-49 and filled with Texas Red dextran through the patch electrode.

(**D**) Pie charts showing the percentage of neurons cultured on IKVAV-PA**2** and laminin coatings that were able to repeatedly fire action potentials.

(**E**) Representative traces of action potentials from human MNs grown on IKVAV-PA**2** and laminin coatings. Action potential size and rate of rise and fall were significantly different for PA**2** versus laminin, see Table S2.

(**F**) Bright-field images of MNs cultured on an MEA plate coated with IKVAV-PA**1** and PA**3** at day 40.

(**G**) Bar graphs showing the number of bursting electrodes (left) and the number of active electrodes (right) per well of hiPSC-derived MN cultures plated on IKVAV-PA and laminin coatings or astrocytic monolayers. Each dot represents values of individual wells from 5 independent differentiations. Asterisks represent significant differences based on ANOVA followed by Tukey's multiple comparison test; **P <0.01 and ****P<0.0001.

Scale bars: **A**=20 μm; **C**= 50 μm; **F**=100 μm**.**

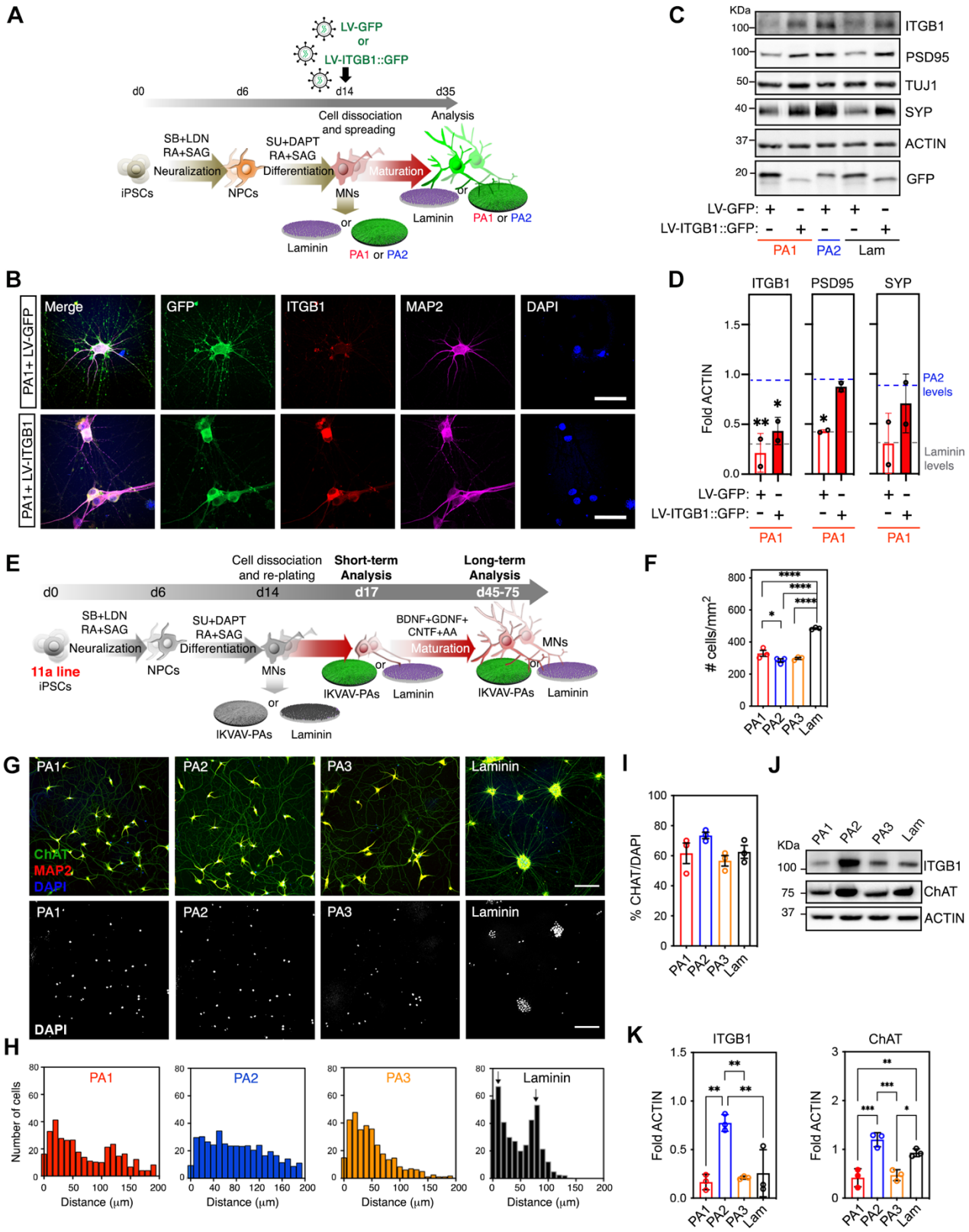
A
LV-GFP
or
LV-ITGB1::GFP
d0
d6
d14
d35
Cell dissociation and spreading
Analysis
SB+LDN
RA+SAG
Neuralization
SU+DAPT
RA+SAG
Differentiation
Maturation
iPSCs
NPCs
MNs
or
Laminin
PA1 or PA2
B
PA1+ LV-GFP
PA1+ LV-ITGB1
Merge
GFP
ITGB1
MAP2
DAPI
C
KDa
100
100
50
40
37
20
ITGB1
PSD95
TUJ1
SYP
ACTIN
GFP
LV-GFP: + - + + -
LV-ITGB1::GFP: - + - - +
PA1
PA2
Lam
D
ITGB1
PSD95
SYP
Fold ACTIN
1.5
1.0
0.5
0.0
PA2 levels
Laminin levels
LV-GFP: + - + - + -
LV-ITGB1::GFP: - + - + - +
PA1
PA1
PA1
E
Cell dissociation and re-plating
Short-term Analysis
Long-term Analysis
d0
d6
d14
d17
d45-75
SB+LDN
RA+SAG
Neuralization
SU+DAPT
RA+SAG
Differentiation
BDNF+GDNF+
CNTF+AA
Maturation
11a line
iPSCs
NPCs
MNs
or
IKVAV-PAs
Laminin
F
cells/mm2
800
600
400
200
0
****
****
****
*
PA1
PA2
PA3
Lam
G
PA1
PA2
PA3
Laminin
ChAT
MAP2
DAPI
H
Number of cells
PA1
PA2
PA3
Laminin
Distance (μm)
I
% CHAT/DAPI
100
80
60
40
20
0
PA1
PA2
PA3
Lam
J
KDa
PA1
PA2
PA3
Lam
100
75
37
ITGB1
ChAT
ACTIN
K
ITGB1
ChAT
Fold ACTIN
1.5
1.0
0.5
0.0
3
2
1
0
**
**
**
***
***
*
PA1
PA2
PA3
Lam

Figure S6, related to Figure 6. The Modulation of ITGB1 Expression by the Highly Mobile IKVAV-PA2 Triggers Changes in Cellular Behavior.

(**A**) Schematic representation of the experimental workflow with hiPSC-derived MNs cultured on IKVAV-PA**1**, PA**2** or laminin coatings and transduced with LV-GFP, or ITGB1-GFP lentiviruses.

(**B**) Representative confocal images of hiPSC-derived MNs cultured on IKVAV-PA**1** and transduced with LV-GFP or ITGB1-GFP lentiviruses. Cells were labeled with GFP (green) and stained for ITGB1 and MAP2 (magenta). Nuclei were labeled with DAPI (blue).

(**C**) Representative WB of ITGB1, TUJ1 and synaptic proteins (PSD95, SYP) from MN cultures on IKVAV-PA**1**, PA**2** or laminin coatings and transduced with LV-GFP or ITGB1-GFP lentiviruses. GFP was used to determine transduction efficiencies and ACTIN was used as a loading control.

(**D**) Bar graphs representing the normalized protein levels of ITGB1, PSD95 and SYP in human MNs cultured on IKVAV-PA**1** and transduced with LV-GFP or ITGB1-GFP lentiviruses. Blue and gray dashed lines indicated mean protein levels in PA**2** or laminin coatings, respectively. All values were normalized to ACTIN. Asterisks represent significant differences relative to PA**2** coatings based on ANOVA followed by Tukey's multiple comparison test; *P <0.05 and **P<0.01.

(**E**) Schematic representation of the experimental paradigm of 11a hiPSC line-derived MNs cultured on IKVAV-PAs and commercial laminin coatings.

(**F**) Bar graph representing the number of cells per mm^2 in 11a line hiPSC-derived MN cultures on IKVAV-PAs and laminin coatings at 72h. Asterisks represent significant differences based on ANOVA followed by Tukey's multiple comparison test; *P <0.05 and ****P<0.0001.

(**G**) Representative confocal micrographs of 11a line hiPSC-derived MN cultures plated on the various coatings after >45 days. Cells were stained with neuronal (MAP2, red) and MN (ChAT, green) markers (top row). Nuclei were stained with DAPI (bottom row).

(**H**) Histogram analysis of cell distribution on the different coatings as referred to in **G**.

(**I**) Bar graph representing the percentage of ChAT+ cells in 11a line hiPSC-derived MN cultures on IKVAV-PAs and laminin coatings >45 days. No significant differences were observed across conditions based on ANOVA followed by Tukey's multiple comparison test.

(**J**) Representative WB of ITGB1 receptor and ChAT from 11a line hiPSC-derived MN cultures on IKVAV-PAs and laminin coatings >45 days. ACTIN was used as a loading control.

(**K**) Bar graphs showing normalized protein levels of ITGB1 and ChAT in the 4 tested experimental conditions. All values were normalized to ACTIN. Asterisks represent significant differences based on ANOVA followed by Tukey's multiple comparison test; *P <0.05, **P<0.01 and ***P<0.001.

Data was obtained from at least 3 independent differentiations, except for PA**1** condition in **A**-**D** that was obtained from 2 distinct differentiations. All the values are presented as the mean ± SEM. Each dot in the graphs represents values from independent differentiations. Scale bars: **B**=50 μm; **G**= 100 μm.

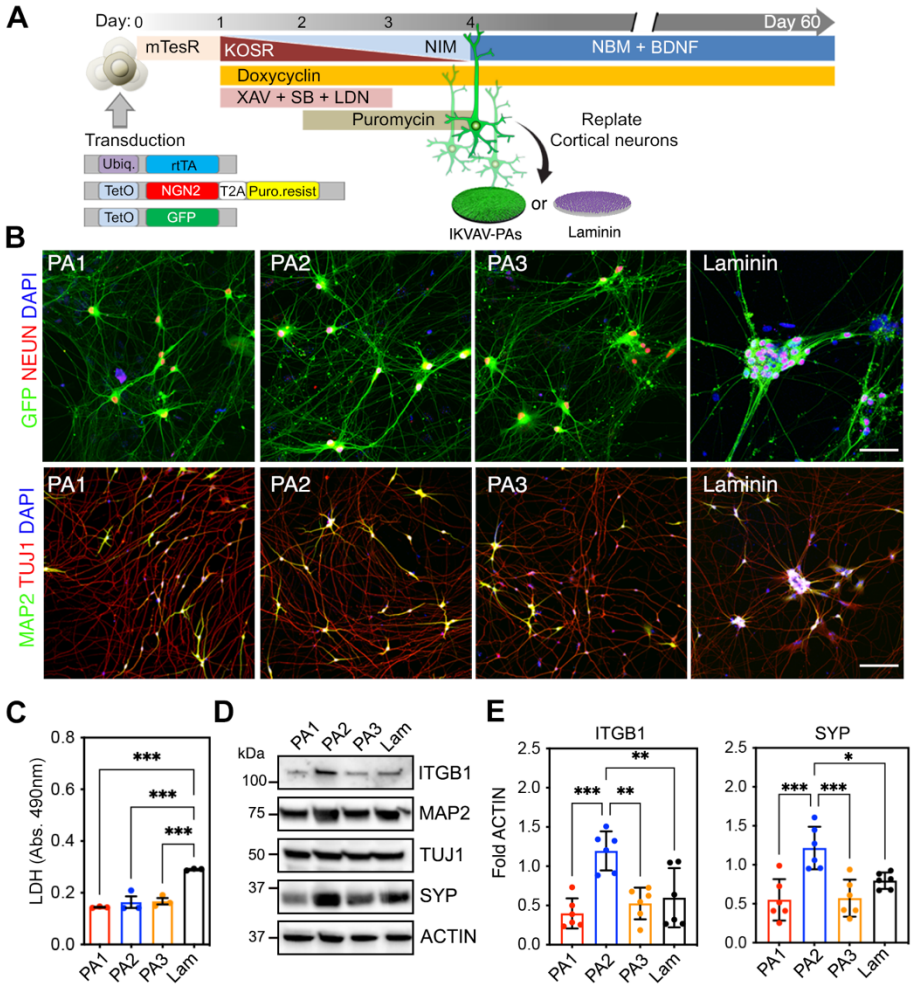

Figure S7, related to Figure 6. Highly Mobile IKVAV-PA Supramolecular Scaffold Enhances Maturation of Human iPSC-Derived Cortical Excitatory Neurons.

(**A**) Schematic representation of cortical neuron differentiation from hiPSC, and culture on IKVAV-PA scaffolds or laminin coatings.

(**B**) Representative confocal micrographs of hiPSC-derived cortical neurons cultured on the different IKVA-PAs and on laminin coatings at day 60. Cells were stained with the neuronal markers TUJ1, MAP2, and NEUN. Nuclei were stained with DAPI. Scale bars: Top=50 μm; Bottom=100 μm.

(**C**) Bar graph representing the released LDH levels in hiPSC-derived cortical neurons after 72h on PA**1**, PA**2**, PA**3,** and commercial laminin coatings. Asterisks represent significant differences based on ANOVA followed by Tukey's multiple comparison test; ***P<0.001.

(**D**) WB of ITGB1 receptor, neuronal markers MAP2 and TUJ1, and the synaptic marker SYP in cortical neurons cultured on IKVAV-PAs or commercial laminin coatings. ACTIN was used as a loading control.

(**E**) Bar graphs showing the normalized protein levels of ITGB1 and SYP in the 4 tested experimental conditions. All values were normalized to ACTIN. Asterisks represent significant differences based on ANOVA followed by Tukey's multiple comparison test; *P <0.05, **P<0.01 and ***P<0.001.